HHS Public Access

Author manuscript

Nat Immunol. Author manuscript; available in PMC 2016 December 06.

Published in final edited form as:

Nat Immunol. 2016 August ; 17(8): 966–975. doi:10.1038/ni.3483.

Human memory T cells with a naïve phenotype accumulate with aging and respond to persistent viruses

Vesna Pulko[1,2], **John S. Davies**[1,2], **Carmine Martinez**[1,2], **Marion C. Lanteri**[3], **Michael P. Busch**[3], **Michael S. Diamond**[4,5,6], **Kenneth Knox**[1,7], **Erin S. Busch**[8], **Peter A. Sims**[8,9,10], **Shripad Sinari**[11], **Dean Billheimer**[11], **Elias K. Haddad**[12], **Kristy O. Murray**[13,14,15], **Anne M. Wertheimer**[1,2], and **Janko Nikolich-Žugich**[1,2,7,#]

[1]Department of Immunobiology, University of Arizona College of Medicine, Tucson, AZ

[2]Arizona Center on Aging, University of Arizona College of Medicine, Tucson, AZ

[3]Blood Systems Research Institute, San Francisco, CA

[4]Department of Medicine, Washington University, St. Louis, MO

[5]Department of Molecular Microbiology, Washington University, St. Louis, MO

[6]Department of Pathology and Immunology, Washington University, St. Louis, MO

[7]Department of Medicine, University of Arizona College of Medicine, Tucson, AZ

[8]Department of Systems Biology, Columbia University Medical Center, New York, NY

[9]Department of Biochemistry & Molecular Biophysics, Columbia University Medical Center, New York, NY

[10]Sulzburger Columbia Genome Center, Columbia University Medical Center, New York, NY

[11]Statistics Consulting Laboratory, Bio5, University of Arizona, Tucson AZ

[12]Division of Infectious Diseases and HIV Medicine, Drexel University College of Medicine, Philadelphia, PA

[13]Department of Pediatrics, Baylor College of Medicine, Houston, TX

[14]National School of Tropical Medicine, Baylor College of Medicine, Houston, TX

[#]to whom correspondence should be addressed at Nikolich@email.arizona.edu, or at Box 245221, 1501 N. Campbell Ave, Tucson, AZ, 85724, USA.

AUTHOR CONTRIBUTION STATEMENT: VP and JNŽ designed and analyzed experiments. VP performed stimulation analysis, cell sorting and RNA isolation. JSD performed flow cytometry and SPADE analysis. CM KOM and AMW performed subject consenting, blood draws, sample organization and human subject database searching and sample management for Arizona, Oregon and Texas subjects. MCL and MPB provided WNV-exposed samples from the San Francisco Blood Bank. MSD facilitated sample transfer. KOM provided WNV-exposed subject samples from the Houston area. KK provided HIV+ subject samples. ESB and PAS performed the RNASeq experiments, and together with VP, JSD, SS and DB, performed RNASeq data analysis. EKH provided subject samples and critical design input. VP and JNŽ wrote the manuscript. JSD, MCL, MPB, MSD, KK, PAS, DB and AWM edited the manuscript. JNŽ conceived the study.

COMPETING FINANCIAL INTERESTS

Authors declare no competing financial interests.

[15]Texas Children's Hospital, Houston, TX

Abstract

The numbers of naive T cells decrease, and the susceptibility to new microbial infections increases with age. Here, we describe a new subset of phenotypically naive human $CD8^+$T cells that rapidly secrete multiple cytokines in response to persistent viral antigens but differ transcriptionally from memory and effector T cells. The frequency of these $CD8^+$T cells, named T memory cells with naïve phenotype (T_{MNP}) increased with age and following severe acute infection and inversely correlated with the residual immune capacity to respond to new infections with age. $CD8^+T_{MNP}$ cells represent a new potential target for immunotherapy of persistent infections, and should be accounted for and subtracted from the naive pool if truly naive T cells are needed to respond to antigens.

Protective immunity against new infections requires sufficient numbers and diversity of naive T lymphocytes (T_N), with strong expansion and effector differentiation potential[1]. With aging, the human T_N cell pool shrinks[2] and may or may not lose diversity[3,4]; and old T_N cells exhibit proliferation and effector differentiation defects[5,6,7,8]. This likely precipitates the vulnerability of older adults to new and re-emerging infections, such as influenza, West Nile virus (WNV), etc. and limits the efficacy of vaccination against infectious diseases[9,10].

Drivers contributing to age-related decline in T_N cell homeostasis and function, include thymic involution[11], impaired peripheral T cell maintenance[12], "homeostatic" conversion to memory phenotype(s)[12] and repeated antigen exposure due to persistent infections[3,13]. However, the extent of quantitative and quantitative age-related decline in T_N function and homeostasis remains incompletely understood.

T cell phenotype has long been used as means to functionally classify T cell subsets (rev. in[14]). For example, naive T cells (T_N) cells exhibit no immediate effector functions[14], whereas T effector + effector memory (T_{E+EM}), T effector memory cells reexpressing CD45RA (T_{EMRA}), and to a lesser extent central memory cells (T_{CM},) cells can rapidly express multiple different effector molecules (cytokines and cytotoxic molecules such as granzymes –Gzm, and perforin) upon antigen stimulation, to enable rapid control of reinfection. T_{CM}, which are less polyfunctional, primarily reside in secondary lymphoid organs and maintain high proliferative potential[15,16]. T memory (T_M) and T_N cells are maintained by interleukin 7(IL-7) and IL-15, respectively[17].

While testing human T cell function across aging, we discovered a subset of phenotypically T_N cells capable of producing effector cytokines immediately upon T cell receptor (TCR) stimulation. These memory T cells with naïve phenotype (which we refer to as T_{MNP}) were dominantly $CD8^+$, exhibited a transcriptome distinct from other T cell subsets and increased in frequency with age. T_{MNP} cells responded to antigens from persistent viruses. They were expanded in patients who experienced symptomatic, but not asymptomatic, WNV infection, months and years following infection, and were the only T cell subset (including T_N, T_{CM}, T_{EM}, and T_{EMRA}) that correlated with symptomatic WNV infection. Therefore, the presence

of $CD8^+T_{MNP}$ cells could be useful in immunotherapy of persistent infections, or should be accounted for if truly naive T cells are needed to respond to antigens.

RESULTS

A subset of phenotypically naive T cells produce cytokines

One key age-related population change in the T cell pool is an absolute numerical decrease of blood $CD8^+T_N$ cells[2]. To investigate whether the peripheral blood $CD8^+T_N$ cells also show qualitatively altered responses with aging, we stimulated peripheral blood mononuclear cells (PBMC, used throughout the study, unless otherwise specified) from 92 subjects (43 males, 49 females, aged 21–97y) with phorbol-myristate acetate (PMA) and calcium ionophore ionomycin(Iono) for 3h and measured intracellular interferon-γ (IFN-γ) cytokine protein production (Fig. 1). Multicolor flow cytometry (FCM) was performed to gate on the four main $CD8^+$ T cell subsets (T_N, T_{CM}, T_{EM}, and T_{EMRA}) defined by CD45RA, CCR7, CD95 and CD28 Thereby, T_N cells were classified as $CD45RA^+CCR7^+CD95^{low}CD28^{int}$; T_{CM} as $CD45RA^-CCR7^+CD95^{hi}CD28^{hi}T_{E+EM}$ as $CD45RA^-CCR7^-CD95^{hi}CD28^{low}$ and T_{EMRA} as $CD45RA^+CCR7^-$ $CD95^{hi}CD28^{low.}$. These definitions were used throughout this study (unless indicated, where full phenotype is provided), because they correlate well with the functional characteristics of different T cell subsets. and in[14] (Supplementary Fig. 1a,b). Total $CD8^+T_N$ numbers declined with aging from >250 cells/μl blood at 20–30y to <50 cells/μl at >80y of age (Fig. 1a, Supplementary Fig. 1c), confirming previous observations[2]. However, following a 3h stimulation with PMA + Iono, 0.2–50% of $CD8^+$ T_N cells produced IFN-γ, in comparison to <0.1% in unstimulated controls and >60% of T_{EM} and T_{EMRA} cells (Fig. 1a). This fraction increased with age, from 2.9 ±1.7% in 21–40y olds, to 8.7±9.9% of $CD8^+T_N$ cells in people >65 y (Fig. 1b). The increase in IFN-$\gamma^+CD8^+T_N$ cells with age was relative; their absolute number also declined with age, albeit less rapidly than the $CD8^+T_N$ cells (Supplementary Fig. 1c). A fraction of PMA+Iono-stimulated $CD4^+T_N$ cells (1–2%) also produced IFN-γ (Supplementary Fig. 1d). Upon PMA+Iono stimulation, freshly isolated PBMCs (n=7, 36–76y) and sorted $CD45RA^+CCR7^+CD95^{hi}CD28^{low}$ $CD8^+T_N$ cells (n=2, 40 and 69y, representative of n=6, 32–76y) produced GzmB (0.06–11.1%), IFN-γ (0.5–16.2%), IL-2 (0.4–3.8%) and TNF (1.8–22.7%); brefeldin A (BfA) background control was <0.37%) (Fig. 1c; Supplementary Fig. 1d,e). This excluded the possibility that the IFN-γ^+CD8^+ cells were T_M cells that acquired a naive phenotype during the freeze-thaw process or PMA+Iono stimulation. IFN-$\gamma^+CD8^+T_N$ cells did not exhibit homogenous expression of CD45RA, CCR7, CD28 and CD95 and were dispersed within the T_N gate (Fig. 1a), showing phenotypic microheterogeneity like other T cell subsets[18]. This suggests that IFN-$\gamma^+CD8^+T_N$ cells are not a contaminating memory population that clusters adjacent to T_M. Thus, a subset of phenotypically $CD8^+T_N$ cells can produce multiple cytokines upon polyclonal stimulation.

T_M cells with naive phenotype (T_{MNP}) are $CD49d^+CXCR3^+$

To assess whether the cytokine-producing $CD8^+T_N$ cells can be distinguished from other T_N cells we used SPADE (cyto-spanning-tree progression of density-normalized events), an unsupervised clustering FCM analysis software. The expression of five T cell activation and

differentiation markers (CD45RA, CCR7, CD95, CD28 and CD45RO) distinguished four canonical T cell subsets (T_N, T_{CM}, $T_{E/EM}$, and T_{EMRA}) amongst the PMA+Iono-stimulated PBMC (Fig. 2a,b). The T_N cell subset was further split into seven nodes, four of which were T_N by the $CD45RA^+CCR7^+CD95^{low}CD28^{int}$ phenotypic definition, and one of whom was enriched for IFN-γ-producing cells (Fig. 2a), suggesting that IFN-$\gamma^+CD8^+T_N$ cells represent a distinct T cell subset.

When scoring the expression of a broader set of markers to stringently define $CD8^+T_N$ cell as $CD27^+CD45RO^-CD127^+CD122^{lo}CD31^+CD11a^-HLA\text{-}DR^-$, IFN-$\gamma^+CD8^+T_N$ cells did not diverge from IFN$\gamma^-CD8^+T_N$ cells, regardless of whether we initially gated through less ($CD45RA^+$ $CCR7^+$) or more stringent ($CD45RA^+CCR7^+CD95^{low}CD28^{int}$) T_N gate (Fig. 3, Supplementary Fig. 2a). However, mean fluorescence intensity (MFI) expression analysis revealed that IFN-$\gamma^+CD8^+T_N$ cells expressed slightly less CCR7 and more CD28 compared to IFN-$\gamma^-CD8^+T_N$ cells; CD45RA and CD95 expression was similar (Supplementary Fig. 2b). The phenotypic profile of IFN-γ^+CD8^+ T_N cells was markedly distinct from T_{CM} and T_{E+EM} cells (Fig. 3b,c, Supplementary Fig. 2). The effector-memory function of IFN-$\gamma^+CD8^+T_N$ cells, along with their naive phenotype, led us to name these cells as memory T cells with naive phenotype(T_{MNP}). We next analyzed trafficking and adhesion receptors on T_{MNP} cells. CD49d, the α_4 integrin, associates with β subunits to form $\alpha_4\beta_7$ or $\alpha_4\beta_1$ heterodimers that regulate effector-memory T cell trafficking[19]. In mice, CD49d exclusively marks antigen-experienced T_M cells[20]. IFN-$\gamma^+CD45RA^+CCR7^+CD95^{low}CD28^{int}CD8^+T_{MNP}$ cells consistently expressed the most CD49d compared to T_N, T_{CM}, T_{EM}, and T_{EMRA}, on average a 2.5-fold higher CD49d geometric MFI (gMFI) than the IFN-$\gamma^-CD8^+T_N$ cells (Fig. 3c,d). However, while all IFN-$\gamma^+CD8^+T_{MNP}$ cells were $CD49d^{hi}$, <10% $CD49d^{hi}CD8^+T_N$ cells did not produce IFN-γ, suggesting that CD49d highly enriches, but not exclusively identify, $CD8^+T_{MNP}$ cells. IFN-$\gamma^+CD45RA^+CCR7^+CD95^{low}CD28^{int}CD8^+T_{MNP}$ cells also expressed the highest ($p<0.0001$ vs T_N cells) levels of the chemokine receptor CXCR3 compared to T_N (defined as IFN-$\gamma^-CD45RA^+CCR7^+CD95^{low}CD28^{int}$), T_{CM}, T_{EM}, and T_{EMRA} (Fig. 3c,d), suggesting the capacity to respond rapidly to CXCL9, CXCL10 and CXCL11, which would direct them to inflamed sites[21]. Because CD49d and CD103 (α_E integrin) can both bind β7 integrin, and because CD103/β7 heterodimer directs immune cell trafficking to tissue residence, including gut mucosa[22,23] we tested expression of CD103, which was comparably low on $CD8^+T_{MNP}$ and $CD8^+T_N$ cells (Fig. 3c), suggesting that these cells are unlikely to home to gut mucosa. Therefore, while $CD8^+T_{MNP}$ cells possess most of the $CD8^+T_N$ phenotypic attributes, they exhibit rapid functional responses and have the potential to traffic to inflamed sites.

T_{MNP} cells are preactivated due to Erk phosphorylation

To determine whether $CD8^+T_{MNP}$ cells respond to TCR-mediated activation, we stimulated PBMC (n=5, 33–77y) for 3h with plate-bound anti-CD3, and soluble anti-CD28 ±anti-CD49d Ab. TCR crosslinking induced production of IFN-γ, TNF and GzmB in $CD49d^{hi}CD45RA^+CCR7^+CD95^{low}CD28^{int}$ $CD8^+T_{MNP}$ cells, although the frequency of IFN-$\gamma^+CD8^+T_{MNP}$ cells was 20–30% of that induced by PMA+Iono (Fig. 4a). Anti-CD49d antibodies did not affect the magnitude (Fig. 4a), breadth or kinetics of cytokine production

(not shown). Therefore, CD49d engagement does not costimulate production of IFN-γ, TNF-α and GzmB in $CD8^+T_{MNP}$ cells.

Polyfunctionality of $CD8^+T_{MNP}$ cells, measured as simultaneous production of IFN-γ, GzmB and TNF in response to stimulation, was similar to that of $CD8^+T_{EMRA}$ cells (Fig. 4b), as T_{MNP} and T_{EMRA} produced all three cytokines (50–60%), TNF only (20–25%), and TNF+IFN-γ (15–25%) at comparable frequencies to $CD8^+T_{EMRA}$ cells, as opposed to T_{CM} (~50% TNF^+ single producers) and T_{EM} (>40% $TNF^+IFN\text{-}\gamma^+$ cells) (Fig. 4b). Therefore, $CD8^+T_{MNP}$ cells were highly polyfunctional. Moreover, about 40% of the $IFN\text{-}\gamma^+GzmB^+CD8^+T_{MNP}$ cells also expressed perforin (Fig. 4c) and all of the $IFN\text{-}\gamma^+GzmB^+CD8^+T_{MNP}$ cells were $CD107a^+$ and thus were functionally lytic (Fig. 4c). Therefore, $CD8^+T_{MNP}$ cells were in a differentiated, polyfunctional state that contrasts with the quiescent, effector molecule-negative $CD8^+T_N$ cells.

We next FCM-sorted $CD49d^{hi}CD45RA^+$ $CCR7^+CD95^{lo}CD28^{int}CD8^+T_{MNP}$ cells and compared their proliferation to $CD49d^{lo}CD45RA^+CCR7^+CD95^{lo}CD28^{int}CD8^+T_N$, T_{CM} and T_{EM} cells in response to the homeostatic cytokines IL-7 and IL-15. $CD8^+T_{MNP}$ cells divided more in the presence of IL-7 or IL-7+ IL-15 than $CD8^+T_N$ cells (Fig. 4d; n=2, 35 and 67y, of n=8). In contrast to $CD8^+T_N$ cells and similar to T_{CM} and T_{EM} subsets, $CD8^+T_{MNP}$ cells also proliferated in response to IL-15 alone (Fig. 4d), which is a cardinal characteristic of T_M cells. When incubated with IL-15 for >3 days, $CD49d^{hi}CD8^+T_{MNP}$ cells lost CCR7 and CD45RA expression faster than $CD8^+T_N$ cells (Fig. 4e). Regardless of that, CD122 (IL-15Rβ) expression was similar between $CD8^+T_{MNP}$ ($CD49^{hi}$-sorted T_N) and $CD8^+T_N$ ($CD49^{lo}$-sorted T_N; both $CD45RA^+CCR7^+CD95^{lo}CD28^{int}$) (Fig. 3b, Supplementary Fig. 2.). Finally, $CD49^{hi}CD45RA^+CCR7^+CD95^{lo}CD28^{int}CD8^+T_{MNP}$ cells did not secrete IFN-γ in response to overnight stimulation with IL-12+IL-18, suggesting that they cannot undergo Ag-nonspecific, bystander responses typical of other T_M cells[24] (Supplementary Fig. 3a,b).

The above results suggested that T_{MNP} cells could be partially activated via TCR. We therefore tested intracellular expression of T-bet (n=9, 24–78y) and of phosphorylated Akt and ERK kinases (n=7, 35–83y) in FCM-identified $CD49d^{hi}CD45RA^+$ $CCR7^+CD95^{lo}CD28^{int}CD8^+T_{MNP}$ and $CD49d^{lo}CD45RA^+CCR7^+CD95^{lo}CD28^{int}CD8^+T_N$ cells, and compared it to $T_{CM,}$ T_{EM} and T_{EMRA} $CD8^+$ cells. Expression of T-bet, master transcription factor of T_H1 cells[25,26], was increased significantly in $CD8^+T_{MNP}$ cells compared to $CD8^+T_N$ cells both in the steady-state ($p<0.01$) and following brief PMA+Iono activation ($p<0.001$; Fig. 4f), and was not different (p=not significant) from T_{CM} cells (Fig. 4f). Akt and MAPK (Erk) kinases integrate multiple signaling cascades in T cells. We found no differences in pAKT levels between T_{MNP} and T_N cells (not shown). $CD8^+T_{MNP}$ cells exhibited increased p-ERK at baseline compared to T_N cells, and the difference increased following PMA+Iono stimulation ($p<0.05$; Fig. 4g). Pre-incubation of $CD8^+T_{MNP}$ cells with the Erk inhibitor U0126 decreased their IFN-γ responses to PMA+Iono stimulation in a dose-dependent manner (Fig. 4h), indicating that activated Erk pathway in $CD8^+T_{MNP}$ cells mediated rapid cytokine production. No toxicity was observed at any dose of the inhibitor (not shown). Together, this demonstrates that $CD8^+T_{MNP}$ cells are polyfunctional, exhibit cytolytic potential, can respond to IL-15 and constitutively activate the Erk pathway, which enables their capacity for rapid IFN-γ responsiveness.

T_{MNP} cells have long telomeres and unique transcriptome

To explore whether $CD8^+T_{MNP}$ cells were partially activated $CD8^+T_N$ cells or differentiated $CD8^+T_M$ cells that re-expressed naive markers, we evaluated their proliferative history and transcriptional profile. Telomeres are repeating hexameric sequences of nucleotides at chromosomal ends that provide genomic stability and that shorten with each replication. Telomeres are longer in T_N cells and shorter in T_M subsets[27] and can be used to estimate cell division history. We used multicolored fluorescent in-situ hybridization (flow-FISH) to compare the telomere length in $CD8^+$T cell subsets (defined by CD45RA, CCR7, CD95, CD28 and CD49d as in Supplementary Fig. 4a). Telomere lengths in $CD8^+T_{MNP}$ cells were comparable to those in $CD8^+T_N$ cells (Fig. 5a), suggesting that $CD8^+T_{MNP}$ cells, unlike the other memory subsets, including $CD8^+T_{CM}$, T_{EM} and T_{EMRA}, did not undergo extensive division (Fig. 5a). Therefore, telomere length in $CD8^+T_{MNP}$ cells most closely resembled T_N cells.

We next compared by RNASeq the transcriptome of $CD8^+T_{MNP}$ cells, defined as IFN-γ^+CD45RA$^+$CCR7$^+$CD95^{low}CD28^{int}, to other CD8 T cell subsets (IFN-γ^-CD45RA$^+$CCR7$^+$CD95^{low}CD28^{int} T_N cells; other subsets as above, n=3–5 subjects, 40–76y). Differential gene expression among the T_N, T_{CM}, T_{EM} and T_{EMRA} $CD8^+$T cell subsets (adjusted $p<0.01$, false discovery rate -FDR<0.05; Fig. 5b), was distinguished by principal component (PC)1 variation. The variation captured by PC2 separated the T_{MNP} subset (Fig. 5b), and a combination of PC1 and PC2 variables indicated that T_{MNP} cells were a unique T cell subset (Fig. 5b) with similarities and differences to both $CD8^+T_N$ and $CD8^+T_{CM}$ on one hand and the more differentiated $CD8^+$ T_{EM} and $CD8^+T_{EMRA}$ on the other. A heat map of expression values for genes with the highest contributions to PC1 and PC2 (Fig. 5c) indicated that T_{MNP} clustered the closest to T_N, followed by T_{CM} and further away from T_{EM} and T_{EMRA} subsets (Fig. 5c). The genes that placed the $CD8^+T_{MNP}$ cells outside the canonical $CD8^+T_N$ cluster included the effector genes (e.g. *Ifng*, *Gzmb, Il1b*, *Cxcl3)* and their expression in $CD8^+T_{MNP}$ cells was similar or higher to that observed in $CD8^+T_{CM}$ cells (Fig. 5c). Conversely, genes like *Nkg7, Fasl and Il22* were not expressed in $CD8^+T_{MNP}$ cells and that distinguished them from $CD8^+T_{EM}$ and T_{EMRA} (Fig. 5c). Altogether, transcriptome data suggest that the $CD8^+T_{MNP}$ cells are a unique T cell subset.

$CD8^+$ T_{MNP} cells are highly proliferative

We next explored proliferative potential of $CD8^+T_{MNP}$ cells. We sorted IFN-γ^+CD45RA$^+$ CCR7$^+$CD95^{lo}CD28^{int}$CD8^+T_{MNP}$ cells and their IFN$\gamma^-$$T_N$ counterparts (Suppl. Fig. 5a; n=3; 63,65&68y) or stimulated cells that were then separated by FCM into CD49d^{hi}CD45RA$^+$CCR7$^+$CD95^{lo}CD28^{int}$CD8^+T_{MNP}$, their CD49^{lo}T_N counterparts and T_{CM}, T_{EM} and T_{EMRA} cells (Supplementary Fig. 5b; n=5, 30–80y). Stimulation was for 4h with anti-CD3+anti-CD28 antibodies for Supplementary Fig. 5a, to induce IFN-γ and enable sorting. Cells were stimulated after sort for additional 3 days (Supplementary Fig. 5a) or with no sorting for 6 day (Supplementary Fig. 5b) with anti-CD3+anti-CD2+anti-CD28 antibody-coated beads in 10U IL-2. Division rates, measured using Cell Trace Violet dye dilution, revealed comparable proliferation between $CD8^+T_{MNP}$, $CD8^+T_N$ and T_{CM} cells (Supplementary Fig. 5a). We conclude that, consistent with their long telomeres, T_{MNP} cells possess robust proliferative potential.

T_{MNP} cells respond to persistent viruses

We next examined TCR diversity of $CD8^+T_{MNP}$ by FCM using 24 Ab specific for the TCR β-chain variable region (TCR Vβ), covering 70% of the total TCRVβ repertoire. Compared to $CD49d^{lo}$ $CD45RA^+CCR7^+CD95^{lo}28^{int}CD8^+T_N$, $CD49d^{hi}CD45RA^+CCR7^+CD95^{lo}28^{int}CD8^+T_{MNP}$ cells showed a restricted distribution of TCR Vβ segments, similar to the highly differentiated $CD8^+T_{EMRA}$ cells (Fig. 6a; n=3/11 shown; 24–80y). This suggested that $CD8^+$ T_{MNP} cells could arise in response to antigens that drive the generation of the $CD8^+T_{EM}$ and $CD8^+T_{EMRA}$, rather than due to broad, cytokine-driven memory conversion. Longitudinal comparison of $CD8^+T_{MNP}$ TCR Vβ profile in a representative 50y old subject (of n=2, 50 and 73y) over 24 months showed a stable dominant TCR Vβ14 clonal expansion (Supplementary Fig. 6), suggesting that $CD8^+T_{MNP}$ cells are stably maintained by TCR-driven signals.

$CD8^+T_{EMRA}$ cells are often specific for persistent viruses[28]. To assess whether the $CD8^+T_{MNP}$ cells shared that specificity, we stimulated PBMC (n=8 subjects, 24–80y) for 3h with overlapping 15-mer peptides covering the length of viral proteins. In a representative 66y old donor T_{MNP} cells made up 8.5% of the total response against the Epstein-Barr virus (EBV) BZLF1 protein, and 1.4% of the response against the cytomegalovirus (CMV) pp65, but no response against the influenza A virus (IAV) matrix protein (Fig. 6b). A similar fraction of $CD8^+T_{MNP}$ cells responded to HIV-1 Gag peptide pool in two out of three HIV-infected subjects undergoing HAART therapy, (Fig. 6c). Controls were treated with brefeldin A (negative) or PMA+Iono (positive).

We extended these observations by FCM staining of unstimulated PBMC and identification of Ag-specific cells with peptide-major histocompatibility complex class I (pMHCI) multimers. The majority (>90%) of $CD8^+$T cells specific for HLA-A*0201 bearing immunodominant CMV pp65 NLVPMATM and EBV BMLF1 GLCTLVAML peptides in CMV^+ (n=26) and EBV^+ subjects (n=7), respectively, exhibited the $T_{EM,\ CM\ or\ TEMRA}$ phenotype (Fig. 7a,b). However, phenotypically naïve $CD45RA^+CCR7^+CD95^{lo}CD28^{int}CD8^+$ T cells also bound CMV and EBV pMHCI multimers (Fig. 7a,b,) and a substantial fraction (25% and 12.4% for CMV and EBV, respectively) of them also produced IFN-γ following a 3h stimulation with PMA+Iono (Fig. 7a,b). PMA+Iono stimulation did not induce TCR down-regulation and did not affect pMHC binding (Supplementary Fig. 4b). In contrast, we found no IFN-γ^+CD8^+ cells in the identically gated $CD8^+T_N$ cells that bound pMHCI multimers in CMV- or EBV-negative subjects (Fig. 7a,b). T_{MNP} cells were present at similar frequencies (75% and 67% of $CD45RA^+CCR7^+CD95^{lo}CD28^{int}CD8^+$cells that bound pMHC multimers) in two subjects that had tenfold different overall T cell responses to EBV (Fig. 7b). These results suggest that the $CD8^+T_{MNP}$ cells arise as a part of a response to persistent viral antigens.

To test whether the $CD8^+$ T_{MNP} cells also respond to acute viral pathogens, we FCM-stained vaccinia virus (VACV) vaccinated, CMV^+ donor PBMC with the CMV pMHC tetramer pp65:HLA-A*0201 and the VACV tetramer CLT:HLA-A*0201. $CD8^+T_{MNP}$ cells, as scored by production of IFN-γ following PMA+Iono stimulation, were found amongst CMV-$pMHC^+$ but not VACV-$pMHC^+$ population (Fig. 7c). We also failed to detect IFN-$\gamma^+CD8^+T_{MNP}$ cells specific for the melanoma self-antigen Melan-A/Mart-1[29] in a healthy,

melanoma-negative subjects (Fig. 7d), where all Melan-A/Mart-1$^+$ cells were CD49d$^-$IFN-γ^- (Fig. 7d). Therefore, CD8$^+$T$_{MNP}$ cells are driven by persistent viral infections and do not respond to vaccine or self-antigens.

CD8$^+$ T$_{MNP}$ cells are linked to past severe infections

Because the size and diversity of naïve T cells pool determines the ability to generate protection against new infections[30,31], we investigated whether the frequency and number of CD8$^+$T$_{MNP}$ cells correlated to the immune fitness against acute infections. We compared the frequency of CD8$^+$T$_{MNP}$ cells amongst T$_N$ cells longitudinally from days 2–90 post-diagnosis, in a cohort of WNV infected subjects who either lacked or presented clinical symptoms, such as fever, meningitis and/or encephalitis. Of the CD45RA$^+$CCR7$^+$CD95^{lo}28^{int} naive phenotype T cells, three asymptomatic subjects (of n=11 shown, 39–92y) had 0.3–1.6% IFN-γ^+CD49d^{hi} and 0.3–5.9% GzB$^+$CD49d^{hi}T$_{MNP}$ cells, whereas three (n=16 analyzed, 43–84 y) symptomatic subjects contained 14.2–20.8% and 12.6–19.8% of these cells, respectively(Fig. 8a, b). Furthermore, the average absolute numbers of CD45RA$^+$CCR7$^+$CD95^{lo}28^{int}IFN-γ^+CD49d^{hi} CD8$^+$T$_{MNP}$ cells were <2,000/10^6 CD8$^+$ and >4,000/10^6 CD8$^+$ cells in asymptomatic and symptomatic patients, respectively (Fig 8c), with no differences in the numbers of CD8$^+$T$_N$, T$_{CM}$, T$_{EM}$ or T$_{EMRA}$ cells (Supplementary Fig. 8). WNV infection resulted in an expansion of CD8$^+$T$_{MNP}$ cells in symptomatic but not asymptomatic subjects, evidenced by an increase in CD8$^+$T$_{MNP}$/10^6 CD8$^+$T cells between d2–7 and d60–90 post-infection (Fig. 8d). This shows that frequency and numbers of T$_{MNP}$ cells positively correlate with the severity of acute viral infection.

DISCUSSION

Here, we characterized a novel subset of T cells that appeared functionally differentiated and activated, but which underwent only minimal phenotypic changes compared to CD8$^+$T$_N$ cells and continued to express molecules associated with a naive T cell state. The frequency of these CD8$^+$T$_{MNP}$ cells increased with aging. They were polyfunctional and exhibited increased baseline phosphorylation of Erk, suggesting that they were receiving TCR-mediated signals. Their skewed TCRVβ utilization and TCR specificity for persistent, but not acute, viruses or vaccines, confirmed that CD8$^+$T$_{MNP}$ cells represent a T cell activation stage that allows persistence of antigen-primed, effector-ready T cells in a nearly-naive state.

We speculate that T$_{MNP}$ cells are functionally imprinted at an early stage of differentiation and propose that they represent a third line of defense against persistent viral infections, behind T$_{EM}$ and T$_{CM}$ cells. Their *in vitro* differentiation with IL-7+IL-15 suggested that CD8$^+$T$_{MNP}$ cells maintain their plasticity and can give rise to cells that resemble CD8$^+$T$_{CM}$, T$_{EM}$ and T$_{EMRA}$ cells. This is consistent with the observation that CD8$^+$T$_{MNP}$ cells did not respond to the inflammatory cytokines IL-12 and IL-18 by IFN-γ production, as would be expected of highly differentiated T$_{EM}$ and T$_{EMRA}$ cells. Their telomere lengths were comparable to that of CD8$^+$T$_N$ cells, suggesting they have not undergone extensive proliferation associated with full effector and memory differentiation. Consistent with all of the above, unsupervised and unbiased analysis of the CD8$^+$T$_{MNP}$ cells transcriptome

classified them as a unique subset, clustering between $CD8^+T_N$ and T_{CM} subsets, further apart from terminally differentiated $CD8^+T_{EM}$ and T_{EMRA}.

T_{MNP} cells were the only $CD8^+$ subset whose numbers and frequency expanded in the course of, and correlated with, symptomatic, severe WNV disease. This could be because acute viral infection led to persistent virus reactivation, or for other reasons that remain to be investigated. Despite this, we do not believe these cells are pathogenic or that they contribute to immune dysfunction in a direct, antigen-specific manner. This is because $CD8^+T_{MNP}$ cells expressed CXCR3 and CD49d, allowing them to traffic rapidly to inflamed tissues and engage in virus control using their polyfunctional secretion of T_{H1} cytokines and cytotoxic granules. However, because their numbers also correlated with deterioration of the naïve T cell pool, they could serve as a biomarker for immune vulnerability. Specifically, their presence in the $CD8^+T_N$ pool could be marker of low T_N fitness due the fact that T_{MNP} cells mask an even more pronounced decrease in $CD8^+T_N$ pool size and diversity, which often manifests as an impaired ability to generate optimal immunity against new infections or immunization[32].

Increasing our knowledge about qualitative and quantitative changes in the aging human immune system could help improve immune interventions for older adults, by stratifying at-risk populations and customizing intervention strategies. Indeed, our understanding of the complexity of T cell subset phenotype and function has greatly increased since the original classification into naïve, effector and memory subsets[15,33]. Technical advances have allowed the identification of new T cell subpopulations[28,34,35]. While numerous (>200) transient populations were observed in a study combining phenotypic, functional and antigen specific tetramer-based markers[18], some of them form functionally defined, stable subsets, such as resident memory T cells[36], T stem cell memory[37], recent thymic immigrants[38], early memory $CD4^+$T cells[39] and self-renewing memory $CD8^+$T cells resistant to chemotherapy[40]. $CD8^+T_{MNP}$ cells add to the complexity of the primary T cell response during aging and to our understanding of the generation of an immune response to persistent viruses. Additional work is needed to address whether the T_{MNP} developmental fate intersects with any of the above subsets. In that regard, it will be of interest to directly compare $CD8^+T_{MNP}$ cells with the $CD8^+T_{SCM}$ cells[37], even if indirect comparisons[37, this study] suggest important differences in expression of CD95, CD11a, CD122, CD31, proliferation history and specificity, where T_{SCM}, unlike T_{MNP}, cells respond to acute infections[37].

Overall, $CD8^+T_{MNP}$ cells should be considered when developing immune interventions that rely on the naïve T cell pool[41]. These cells could be useful if immunotherapy is aimed at targeting persistent infections, or should be accounted for if truly naïve T cells are needed to respond to antigens.

PUBLIC DATA AVAILABILITY

RNASeq data set described in Fig. 5 is available to public via the National Library of Medicine Gene Expression Omnibus at http://www.ncbi.nlm.nih.gov/geo/under the accession number GSE80306. Raw data for all other results shown in the manuscript will be

available via the NIAID ImmPort database at http://immport.org/immport-open/public/study/study/displayStudyDetail/SDY736".

ONLINE METHODS

Study Subjects and Blood Samples

This study was approved by the Institutional Review Boards at the University of Arizona (Tucson, AZ; # 080000673), the Oregon Health and Science University (Portland, OR; # IRB00003007), the University of Texas HSC at Houston (Houston, TX), the Vaccine and Gene Therapy Institute-Florida (Port St. Lucie, FL) and the Blood Systems Research Institute (San Francisco, CA). Human samples were obtained from healthy donors, age 21–101 y of age, as indicated in each experiment, recruited at the OHSU, the University of Arizona or the Martin Health system (Florida) over the period of 6 years. Exclusion criteria included known immunosuppressive pathology, stroke, cancer, or use of steroids within the last 5 years. WNV infected donors were enrolled by Blood Systems Research Institute (BSRI) between 2009 and 2011 or by the University of Texas at Houston, between 2006–2009. Samples, demographics and symptoms data were collected and analyzed as previously described [42] after the subjects provided an informed consent approved by the UCSF Committee on Human Research (protocol # 10-01255) or the Committee for the Protection of Human Subjects at the University of Texas Health Science Center at Houston (HSC-SPH-03-039), respectively. Exclusion criteria included known immunosuppressive status, stroke, cancer, or the use of steroids within the last 5 years. Blood was drawn into heparinized Vacutainer CPT tubes (BD Bioscience, Franklin Lakes, NJ) and processed fresh at respective sites per manufacturer's recommendations to isolate peripheral blood mononuclear cells (PBMC) and plasma; K_2-EDTA tubes were used to determine complete blood counts. Peripheral blood mononuclear cells were also isolated from leukapheresis using Ficoll-Paque (GE Healthcare, NJ, USA) density gradient media. PBMCs were frozen in 90% fetal bovine serum (FBS) and 10% DMSO. Initial observational experiment (Fig. 1a,b) was performed on subjects selected randomly to meet age criteria and ensured adequate power, as described in our previous work [2]. Unless stated otherwise, subsequent experiments were performed using subgroups of subjects defined by age and >5% naïve T cell responsiveness measured in Fig. 1a,b) and selected by A.M.W. randomly based on these criteria, without input of V.P., who did the experiments. In these studies, we initially did not observe, and subsequently did not follow, sex differences in T_{VN} cell abundance. Experiments, data collection and Flow Jo analysis were performed blindly up to the point of final analysis as samples associated specific subject ID did not contain information about their age.

Antibodies, Flow Cytometry and Cell Sorting

All antibodies, dilutions and validation are provided in Supplementary Table 1. TCR-Vβ specificity was evaluated by IOTest® Beta Mark Kit (Beckman Coulter). HLA-A2 CMV-NLV, HLA-A2 VV-CLT, and HLA-A2 Melan-A-ELA tetramers were obtained from the NIH tetramer core facility at Emory University, HLA-A2 INF-GIL tetramers were generously provided by Dr. K. Kedzierska's laboratory at the University of Melbourne, Melbourne,

Australia and HLA-A2 EBV-GLC dextramers were obtained from IMMUDEX (Copenhagen, Denmark).

Frozen PBMCs were thawed in RPMI medium supplemented with 10% FBS, penicillin and streptomycin in the presence of DNAse (Sigma, Saint Louis, MO), rested overnight in X-Vivo medium (Lonza/Basel, Switzerland) supplemented with 5% human male AB serum and used for surface and intracellular staining at $1–3 \times 10^6$ per sample. Cells were first stained with LIVE/DEAD® Fixable Dead Cell Stain (Life technologies, Eugene, OR), and next incubated with various combinations of antibodies against T cell markers (both for 30 min at 4°C). Tetramers were added 30 min prior to antibodies against other surface markers. For intracellular staining, cells were permeabilized with FACS Permeabilization solution (BD Biosciences or eBiosciences) and incubated with antibodies against various intracellular molecules for 30 min at 4°C. Flow cytometry acquisition was performed on a custom-designed BD Biosciences Fortessa and analyzed using FlowJo software (Tree Star, Ashland, OR). T cell subsets were sorted using a modified FACSAria (BD Biosciences).

Stimulation Assays

PBMCs were stimulated with either PMA/Iono (Cell stimulation cocktail, eBioscience), plate-bound CD3/CD49d/soluble CD28 (at 10 μg/mL, 5 μg/mL, and 5 μg/mL respectively) or with peptides or their mixtures [Influenza Matrix $peptide_{57–66}$ (AnaSpec, San Jose, CA), EBV BZLF-1 peptide pool, CMV pp65 peptide pool (both Miltenyi Biotec, San Diego, CA) or HIV-1 PTE Gag peptide pool[43] (obtained from the NIH AIDS reagent program)] for 3 hrs in the presence of brefeldin A (eBioscience). All peptides were used according to manufacturer's instructions at approximately 1 μg/mL of each peptide; peptide mixtures were constructed as sets of 15-mers overlapped by 9 amino acids. Phenotype and cytokine production were evaluated by flow cytometry as described above. In the phospho ERK blocking experiment, MAPK inhibitor U0126 (Tocris Bioscience, Bristol, UK) was added to PBMCs for 3 h prior stimulation with PMA/Iono.

Phos-Flow

PBMCs were stimulated with PMA/Ionomycin for 5, 10 or 15 min and simultaneously stained with antibodies against surface markers and phospho-Erk (Thr202/Tyr204) using BD Biosciences Phos-flow fixation and permeabilization solutions according to manufacturer's protocol.

Cytokine Proliferation Assays

PBMCs were thawed, labeled with Cell trace violet (CTV) proliferation dye (Molecular Probes, Eugene, OR) according to manufacturer's instructions (2 μM at 5×10^6 cells/mL for 30 min at 37°C) and rested over night. The next day, various T cell subsets were isolated by cell sorting and incubated in the presence of cytokines [IL-7 (50 ng/mL), IL-15 (50 ng/mL) (both R&D Systems, Minneapolis, MN), IL-12 (5 ng/mL; Peprotech, Rocky Hill, NJ) or IL-18 (5 ng/mL; Life Technologies, Eugene, OR)]. On day 3 or 7, phenotype, proliferation (dilution of CTV proliferation dye) and/or cytokine production were evaluated by flow cytometry.

Sorting of IFNγ$^+$ Secretion Assay

PBMCs were thawed, labeled with CTV and rested overnight. The next day, phenotypically naïve IFNγ producing cells ($\mathbf{T_{VN}}$) and nonproducing ($\mathbf{T_N}$) CD8$^+$ T cells were isolated using an IFNγ secretion assay cell enrichment and detection kit (Miltenyi Biotec) and cell sorting. Briefly, cells were transferred onto CD3 coated plates (10 μg/mL; in the presence of soluble CD28 at 5 μg/mL), stimulated for 3 h at 37°C, labeled with IFNγ specific capture antibody reagent and incubated for 45 min at 37°C (while slowly rotating). Next, the cells were concurrently incubated with IFNγ detection antibody and antibodies against the remaining phenotypic T cell markers, which allowed for identification of naive T cell subset. IFNγ producing and nonproducing naïve CD8$^+$ T cell subsets were isolated by cell sorting and incubated in the presence of CD3/CD2/CD28 coated beads (T cell activation/expansion kit, Miltenyi Biotec) at ratio 1:1 in the presence of IL-2 (100 U/mL) for 3 days, when proliferation and phenotype were evaluated by flow cytometry.

SPADE analysis

Spanning-tree progression analysis of density-normalized events (SPADE) clustering algorithm [44] on the Cytobank.org platform was used to analyze doublet-exclused, alive CD8b$^+$ lymphocytes from nine subjects. This produced an interconnected cluster of nodes, or clusters of connected nodes, that correspond with phenotypically defined CD8 T cell populations.

Multi-color flow-FISH

Experiment was performed according to modified manufacturer's protocol as described by Ridell et al. [45]. Briefly, PBMCs were first stained with LIVE/DEAD® Fixable Dead Cell Stain and then incubated with biotinylated CD28 or directly conjugated antibodies (CD45RA (BV711), CCR7 (FITC), CD3 (BV570), CD95 (BV421), CD49d (BV510), CD8α (BV650)), followed by 15 min incubation with streptavidin-conjugated Cy3. Cells were fixed and permeabilized using FACS Fixation and permeabilization kit (BD Biosciences). Samples were than washed in PBS, fixed in 1mM BS3 (30 min on ice, ThermoFisher Scientific) and quenched with 50mM Tris-HCl in PBS (pH 7.2, 20 min, room temperature). The cells were washed twice; first in PBS, and then in hybridization buffer (70% deionized formamide, 28.5mM Tris-HCl pH7.2, 1.4% BSA and 0.2M NaCl). The samples were subsequently resuspended in hybridization buffer and incubated with of the PNA TelC –Cy5 probe (200 nM, PNA Bio Inc, Thousand Oaks, CA) and heated for 10 min at 82C, rapidly cooled on ice and left to hybridize for 1 hr at room temperature in the dark. Lastly, the samples were washed in post-hybridization buffer (70% deionized formamide, 14.25mM Tris-HCl pH7.2, 0.14% BSA, 0.2M NaCl and 0.14% Tween-20) and in PBS 2% BSA before acquisition on BD Biosciences Fortessa and analyzed using FlowJo software. Unless stated otherwise, chemicals were purchased from Sigma-Aldrich (St. Louis, MO).

RNA sequencing

T cell samples from sorted populations were obtained for genome-wide expression profiling by RNA-Seq. There was a broad range of cell numbers available from the different populations (some samples had down to a few thousand cells), and so a strategy for low-

input RNA-Seq across all of the samples was employed. Trizol extraction was followed by isopropanol precipitation to obtain total RNA. Each total RNA sample was re-suspended in 20 uL of Elution Solution (nuclease-free water supplemented with 0.5 U/uL RNase inhibitor (SUPERase IN, Life Technologies)). To isolate mRNA, LNA-oligo(dT) was used rather than DNA-oligo(dT). LNA is an analog of RNA with a modified sugar backbone that imparts a much higher melting point [46] and therefore facilitates high sensitivity mRNA capture. Biotinylated LNA-Oligo(dT) (Exiqon) was attached to streptavidin-coated superparamagnetic beads (C1 Dynabeads, Life Technologies) in Hybridization Buffer (20 mM Tris pH 8, 1 M NaCl, 0.1% tween-20). After washing the beads three times in Wash Buffer (20 mM Tris pH 8, 50 mM NaCl, 0.1% tween-20) and re-suspending in Hybridization Buffer, 20 uL of beads were added to each total RNA sample and the mixture was incubated for 45 minutes at room temperature on a rotisserie. After washing the beads three times with Wash Buffer and re-suspending in 15 uL of Elution Solution, the bead mixture was heated to 75C for two minutes followed by immediate removal of the supernatant containing purified mRNA.

Strand-specific RNA-Seq libraries were constructed using the template-switching strategy implemented in the SMARTer Stranded RNA-Seq kit (Clontech). mRNA fragmentation reactions were run for four minutes and cDNA was purified twice with size selection beads (Ampure XP, Beckman) prior to PCR enrichment. Libraries were sequenced on an Illumina NextSeq 500 sequencer with 75-base single-end reads. The reads were mapped to the Ensembl GRCh37 human genome and transcriptome annotation (obtained from Illumina iGenomes) using Tophat2 [47] and the uniquely mapped reads associated with each gene using HTseq were counted [46]. Differential expression analysis between different T cell populations was constructed using DESeq2 [48]. Normalization was performed with samples within cell types as biological replicates. The counts were transformed using the regularized log transformation provided in the DESeq2 package as described in [48]. Principal component analysis was done based on all genes annotated from the Consensus Coding Sequence (CCDS) Project[49]. The figures were produced using ggplot2 [50] and gplots [51] packages from R programming language.

Supplementary Material

Refer to Web version on PubMed Central for supplementary material.

Acknowledgments

The authors would like to acknowledge Ms. P. Campbell of the Arizona Cancer Center, Arizona Research Laboratory Flow Cytometry Core Facility for expert sorting and the Arizona Cancer Center Support Grant (NCI - CA 023074) for facility support; NIH Tetramer Facility for outstanding reagent preparation; Dr K. Kedzierska (University of Melbourne) for generous donation of key tetramer reagents; and the members of the Nikolich, Kuhns, Frelinger, Wu and Schenten laboratories at the University of Arizona for insight and helpful discussions. This work was supported by the NIAID contract N01-AI00017, the NHLBI grant RC2HL101 and the NIA grants R01 AG-048021 and P30 AG008017 from the National Institutes of Health and by the Bowman Endowed Professorship in Medical Research to J.N-Ž.

References

1. Jenkins MK, Chu HH, McLachlan JB, Moon JJ. On the composition of the preimmune repertoire of T cells specific for Peptide-major histocompatibility complex ligands. Annu Rev Immunol. 2010; 28:275–294. [PubMed: 20307209]
2. Wertheimer AM, Bennett MS, Park B, Uhrlaub JL, Martinez C, Pulko V, et al. Aging and cytomegalovirus infection differentially and jointly affect distinct circulating T cell subsets in humans. J Immunol. 2014; 192(5):2143–2155. [PubMed: 24501199]
3. Nikolich-Zugich J. Ageing and life-long maintenance of T-cell subsets in the face of latent persistent infections. Nat Rev Immunol. 2008; 8(7):512–522. [PubMed: 18469829]
4. Qi Q, Liu Y, Cheng Y, Glanville J, Zhang D, Lee JY, et al. Diversity and clonal selection in the human T-cell repertoire. Proc Natl Acad Sci U S A. 2014; 111(36):13139–13144. [PubMed: 25157137]
5. Linton PJ, Dorshkind K. Age-related changes in lymphocyte development and function. Nat Immunol. 2004; 5(2):133–139. [PubMed: 14749784]
6. Cambier J. Immunosenescence: a problem of lymphopoiesis, homeostasis, microenvironment, and signaling. Immunol Rev. 2005; 205:5–6. [PubMed: 15882340]
7. Goronzy JJ, Weyand CM. T cell development and receptor diversity during aging. Curr Opin Immunol. 2005; 17(5):468–475. [PubMed: 16098723]
8. Miller RA. Effect of aging on T lymphocyte activation. Vaccine. 2000; 18(16):1654–1660. [PubMed: 10689144]
9. Thompson WW, Shay DK, Weintraub E, Brammer L, Cox N, Anderson LJ, et al. Mortality associated with influenza and respiratory syncytial virus in the United States. JAMA. 2003; 289(2): 179–186. [PubMed: 12517228]
10. Petersen LR, Roehrig JT, Hughes JM. West Nile virus encephalitis. N Engl J Med. 2002; 347(16): 1225–1226. [PubMed: 12270973]
11. Chinn IK, Blackburn CC, Manley NR, Sempowski GD. Changes in primary lymphoid organs with aging. Semin Immunol. 2012; 24(5):309–320. [PubMed: 22559987]
12. Nikolich-Zugich J. Aging of the T cell compartment in mice and humans: from no naive expectations to foggy memories. J Immunol. 2014; 193(6):2622–2629. [PubMed: 25193936]
13. Albright, JF.; Albright, JW. Aging, Immunity and Infection. Humana Press; Totowa: 2003.
14. Maecker HT, McCoy JP, Nussenblatt R. Standardizing immunophenotyping for the Human Immunology Project. Nat Rev Immunol. 2012; 12(3):191–200. [PubMed: 22343568]
15. Sallusto F, Geginat J, Lanzavecchia A. Central memory and effector memory T cell subsets: function, generation, and maintenance. Annu Rev Immunol. 2004; 22:745–763. [PubMed: 15032595]
16. Kaech SM, Wherry EJ, Ahmed R. Effector and memory T-cell differentiation: implications for vaccine development. Nat Rev Immunol. 2002; 2(4):251–262. [PubMed: 12001996]
17. Tan J, Ernst B, Kieper W, LeRoy E, Sprent J, Surh C. Interleukin (IL)-15 and IL-7 Jointly Regulate Homeostatic Proliferation of Memory Phenotype CD8+ Cells but Are Not Required for Memory Phenotype CD4+ Cells. J Exp Med. 2002; 195(12):1523–1532. [PubMed: 12070280]
18. Newell EW, Sigal N, Bendall SC, Nolan GP, Davis MM. Cytometry by time-of-flight shows combinatorial cytokine expression and virus-specific cell niches within a continuum of CD8+ T cell phenotypes. Immunity. 2012; 36(1):142–152. [PubMed: 22265676]
19. Hamann A, Andrew DP, Jablonski-Westrich D, Holzmann B, Butcher EC. Role of alpha 4-integrins in lymphocyte homing to mucosal tissues in vivo. J Immunol. 1994; 152(7):3282–3293. [PubMed: 7511642]
20. Chiu BC, Martin BE, Stolberg VR, Chensue SW. Cutting edge: Central memory CD8 T cells in aged mice are virtual memory cells. J Immunol. 2013; 191(12):5793–5796. [PubMed: 24227783]
21. Xia MQ, Qin SX, Wu LJ, Mackay CR, Hyman BT. Immunohistochemical study of the beta-chemokine receptors CCR3 and CCR5 and their ligands in normal and Alzheimer's disease brains. Am J Pathol. 1998; 153(1):31–37. [PubMed: 9665462]

22. Jaensson E, Uronen-Hansson H, Pabst O, Eksteen B, Tian J, Coombes JL, et al. Small intestinal CD103+ dendritic cells display unique functional properties that are conserved between mice and humans. J Exp Med. 2008; 205(9):2139–2149. [PubMed: 18710932]
23. Gebhardt T, Wakim LM, Eidsmo L, Reading PC, Heath WR, Carbone FR. Memory T cells in nonlymphoid tissue that provide enhanced local immunity during infection with herpes simplex virus. Nat Immunol. 2009; 10(5):524–530. [PubMed: 19305395]
24. Tough DF, Zhang X, Sprent J. An IFN-gamma-dependent pathway controls stimulation of memory phenotype CD8+ T cell turnover in vivo by IL-12, IL-18, and IFN-gamma. Journal of Immunology. 2001; 166(10):6007–6011.
25. Szabo SJ, Kim ST, Costa GL, Zhang X, Fathman CG, Glimcher LH. A novel transcription factor, T-bet, directs Th1 lineage commitment. Cell. 2000; 100(6):655–669. [PubMed: 10761931]
26. Knox JJ, Cosma GL, Betts MR, McLane LM. Characterization of T-bet and eomes in peripheral human immune cells. Front Immunol. 2014; 5:217. [PubMed: 24860576]
27. Hodes RJ, Hathcock KS, Weng NP. Telomeres in T and B cells. NatRevImmunol. 2002; 2(9):699–706.
28. Appay V, Dunbar PR, Callan M, Klenerman P, Gillespie GM, Papagno L, et al. Memory CD8+ T cells vary in differentiation phenotype in different persistent virus infections. Nat Med. 2002; 8(4): 379–385. [PubMed: 11927944]
29. Coulie PG, Brichard V, Van Pel A, Wolfel T, Schneider J, Traversari C, et al. A new gene coding for a differentiation antigen recognized by autologous cytolytic T lymphocytes on HLA-A2 melanomas. J Exp Med. 1994; 180(1):35–42. [PubMed: 8006593]
30. Messaoudi I, Guevara Patino JA, Dyall R, LeMaoult J, Nikolich-Zugich J. Direct link between mhc polymorphism, T-cell avidity and diversity in immune defense. Science. 2002; 298:1797–1801. [PubMed: 12459592]
31. Moon JJ, Chu HH, Pepper M, McSorley SJ, Jameson SC, Kedl RM, et al. Naive CD4(+) T cell frequency varies for different epitopes and predicts repertoire diversity and response magnitude. Immunity. 2007; 27(2):203–213. [PubMed: 17707129]
32. Cicin-Sain L, Messaoudi I, Park B, Currier N, Planer S, Fischer M, et al. Dramatic increase in naive T cell turnover is linked to loss of naive T cells from old primates. Proc Natl Acad Sci U S A. 2007; 104(50):19960–19965. [PubMed: 18056811]
33. Hamann D, Baars PA, Rep MH, Hooibrink B, Kerkhof-Garde SR, Klein MR, et al. Phenotypic and functional separation of memory and effector human CD8+ T cells. The Journal of Experimental Medicine. 1997; 186(9):1407–1418. [PubMed: 9348298]
34. Bendall SC, Nolan GP, Roederer M, Chattopadhyay PK. A deep profiler's guide to cytometry. Trends Immunol. 2012; 33(7):323–332. [PubMed: 22476049]
35. Ornatsky O, Baranov VI, Bandura DR, Tanner SD, Dick J. Multiple cellular antigen detection by ICP-MS. J Immunol Methods. 2006; 308(1–2):68–76. [PubMed: 16336974]
36. Schenkel JM, Masopust D. Tissue-resident memory T cells. Immunity. 2014; 41(6):886–897. [PubMed: 25526304]
37. Gattinoni L, Lugli E, Ji Y, Pos Z, Paulos CM, Quigley MF, et al. A human memory T cell subset with stem cell-like properties. Nat Med. 2011; 17(10):1290–1297. [PubMed: 21926977]
38. Haines CJ, Giffon TD, Lu LS, Lu X, Tessier-Lavigne M, Ross DT, et al. Human CD4+ T cell recent thymic emigrants are identified by protein tyrosine kinase 7 and have reduced immune function. J Exp Med. 2009; 206(2):275–285. [PubMed: 19171767]
39. Song K, Rabin RL, Hill BJ, De Rosa SC, Perfetto SP, Zhang HH, et al. Characterization of subsets of CD4+ memory T cells reveals early branched pathways of T cell differentiation in humans. Proc Natl Acad Sci U S A. 2005; 102(22):7916–7921. [PubMed: 15905333]
40. Turtle CJ, Swanson HM, Fujii N, Estey EH, Riddell SR. A distinct subset of self-renewing human memory CD8+ T cells survives cytotoxic chemotherapy. Immunity. 2009; 31(5):834–844. [PubMed: 19879163]
41. Hinrichs CS, Borman ZA, Cassard L, Gattinoni L, Spolski R, Yu Z, et al. Adoptively transferred effector cells derived from naive rather than central memory CD8+ T cells mediate superior antitumor immunity. Proc Natl Acad Sci U S A. 2009; 106(41):17469–17474. [PubMed: 19805141]

42. Lanteri MC, Lee TH, Wen L, Kaidarova Z, Bravo MD, Kiely NE, et al. West Nile virus nucleic acid persistence in whole blood months after clearance in plasma: implication for transfusion and transplantation safety. Transfusion. 2014; 54(12):3232–3241. [PubMed: 24965017]

43. Betts MR, Ambrozak DR, Douek DC, Bonhoeffer S, Brenchley JM, Casazza JP, et al. Analysis of total human immunodeficiency virus (HIV)-specific CD4(+) and CD8(+) T-cell responses: relationship to viral load in untreated HIV infection. JVirol. 2001; 75(24):11983–11991. [PubMed: 11711588]

44. Qiu P, Simonds EF, Bendall SC, Gibbs KD Jr, Bruggner RV, Linderman MD, et al. Extracting a cellular hierarchy from high-dimensional cytometry data with SPADE. Nature Biotechnology. 2011; 29:886–891.

45. Riddell NE, Griffiths SJ, Rivino L, King DCB, Teo GH, Henson SM, et al. Multifunctional cytomegalovirus (CMV)-specific CD8(+) T cells are not restricted by telomere-related senescence in young or old adults. Immunology. 2015; 144:549–560. [PubMed: 25314332]

46. Koshkin AA, Nielsen P, Meldgaard M, Rajwanshi VK, Singh SK, Wengel J. LNA (Locked Nucleic Acid): An RNA Mimic Forming Exceedingly Stable LNA:LNA Duplexes. Journal of the American Chemical Society. 1998; 120:13252–13253.

47. Kim D, Pertea G, Trapnell C, Pimentel H, Kelley R, Salzberg SL. TopHat2: accurate alignment of transcriptomes in the presence of insertions, deletions and gene fusions. Genome Biology. 2013; 14:R36. [PubMed: 23618408]

48. Love MI, Huber W, Anders S. Moderated estimation of fold change and dispersion for RNA-seq data with DESeq2. Genome Biology. 2014; 15:550. [PubMed: 25516281]

49. Pruitt KD, Harrow J, Harte RA, Wallin C, Diekhans M, Maglott DR, et al. The consensus coding sequence (CCDS) project: Identifying a common protein-coding gene set for the human and mouse genomes. Genome Research. 2009; 19:1316–1323. [PubMed: 19498102]

50. Wickham, H. ggplot2: Elegant Graphics for Data Analysis. Springer Science & Business Media; 2009.

51. Warnes GR, Bolker B, Bonebakker L, Gentleman R, Huber W, Liaw A, LumleyMaechler M, Magnusson A, Moeller S, Schwartz M, Venables B. gplots: Various R Programming Tools for Plotting Data. 2015

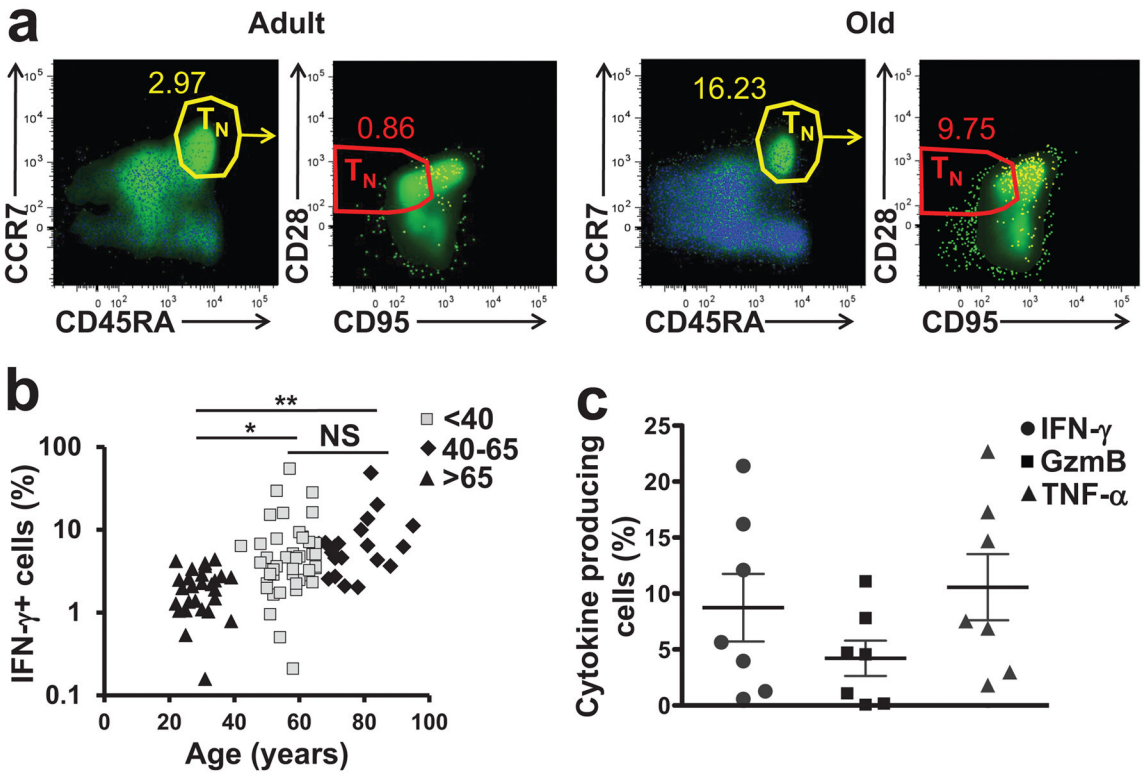

Figure 1. Age-related increase in phenotypically naive T cells capable of rapid cytokine production

(**a**) Intracellular IFN-γ staining of human PMA/iono- activated PBMCs from representative healthy adult, 32 y old, and old, 76 y old, donors. Overlaid dot plots show % of naive $CD45RA^{+}CCR7^{+}$ (yellow gate) and subsequently $CD45RA^{+}CCR7^{+}CD95^{lo}CD28^{int}$ (red gate) CD8 T cells producing IFN-γ^{+} (in blue) overlaid over total $CD8^{+}$ T cells (in green). **b.** Percentage of $CD8^{+}$ naïve phenotype $CD45^{+}CCR7^{+}CD95^{lo}CD28^{int}$ cells producing IFN-γ across age. Data are from one of two experiments. t-test was used to show significance in the increase between the group of 21–40 years old (n=27); 40 – 65 years old (n=44) and 66–97 year old donors (>65 years old; n=21; *p<0.05; **p<0.001). **c.** Bar graph showing cytokine production by phenotypically naive $CD45RA^{+}$ $CCR7^{+}CD95^{lo}CD28^{int}$ $CD8^{+}$ T cells from freshly isolated blood (age 32–76;n=7).

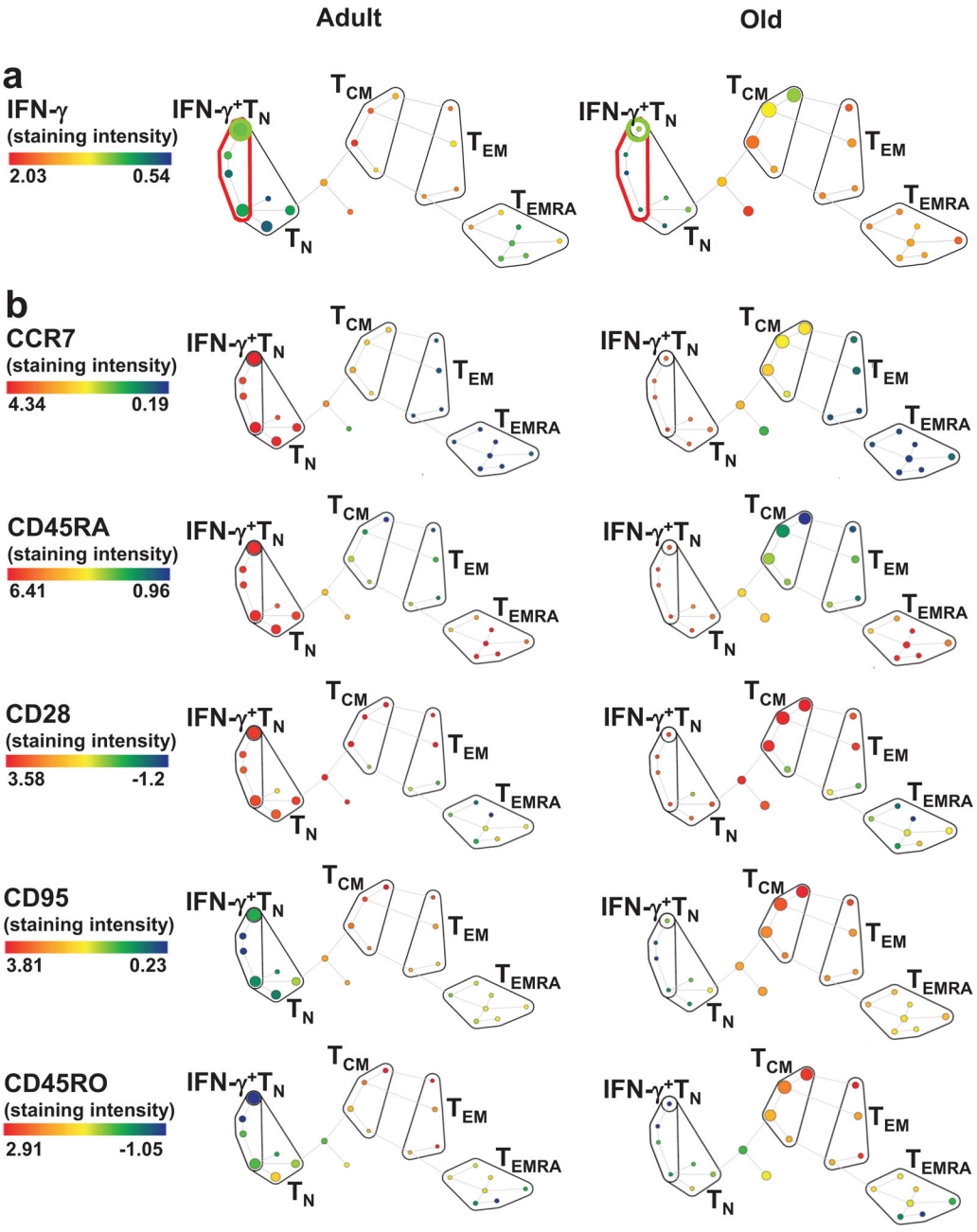

Figure 2. SPADE analysis of CD8$^+$ T cells demonstrates clustering of T_{MNP} cells with T_N group

Two representative subjects (adult, age 27, left; and old, age 68, right) are shown. **a.** IFN-γ producing cells form a unique naive CD8$^+$ T cell subset. Node size depicts the relative count and the color represents IFN-γ staining intensity. Four canonical populations are outlined in black, CD45RA$^+$CCR7$^+$CD95^{lo}CD28^{int}- defined naive population in red, and IFN-γ$^+$ naive population in bright green. **b.** Naive phenotype of IFN-γ producing T_{MNP} CD8$^+$T cells. Colors represent staining intensity of phenotypic markers indicated in the legend. Data are representative of a single experiment (n=9, 6 males, 3 females, age 27–78).

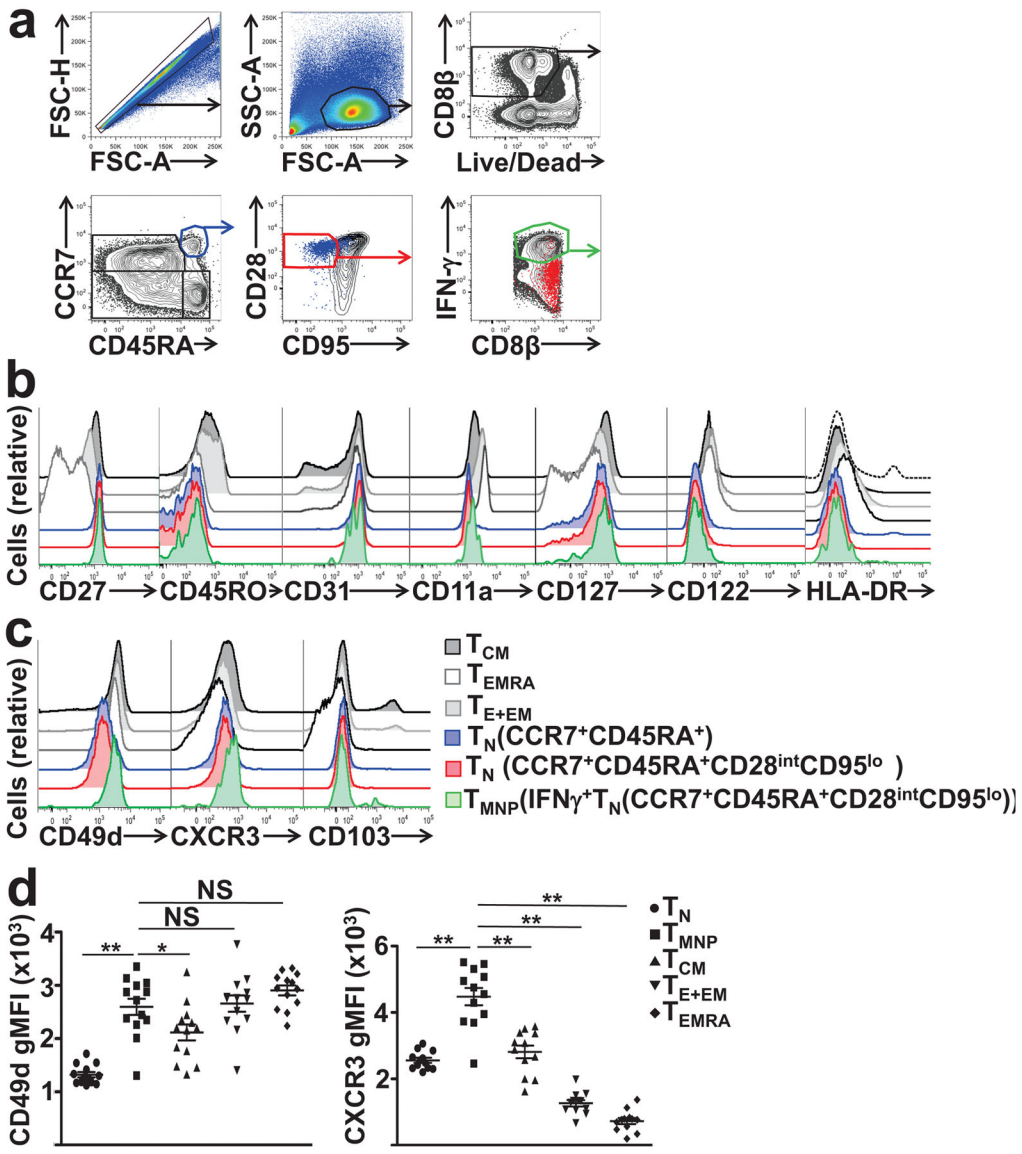

Figure 3. T_{MNP} cells form a unique T cell subset with naive phenotype that expresses higher levels of CD49d and CXCR3

a. Flow cytometry analysis of human PMA/iono-activated PBMCs from a representative donor (age 54). Dot plots show gating strategy used to identify T_{MNP} $CD8^+$ T cells based on the expression of $CD45RA^+$ $CCR7^+CD95^{lo}CD28^{int}$ and IFN-γ production (four canonical populations are outlined on CCR7 vs CD45RA plot). **b,c.** Overlaid histogram plots show expression level [mean geometric mean fluorescence intensity (gMFI) ± standard error of the mean (SEM)] of an indicated surface antigen in different $CD8^+$ T cell subsets from a representative donor from **a. d.** Repeated measures one-way ANOVA was used to quantify differences in CD49d and CXCR3 expression between T_N and T_{MNP} CD8 T cells (*p<0.01,**P<0.001; data are representative of two experiments, n=13 and 12, age 27–85).

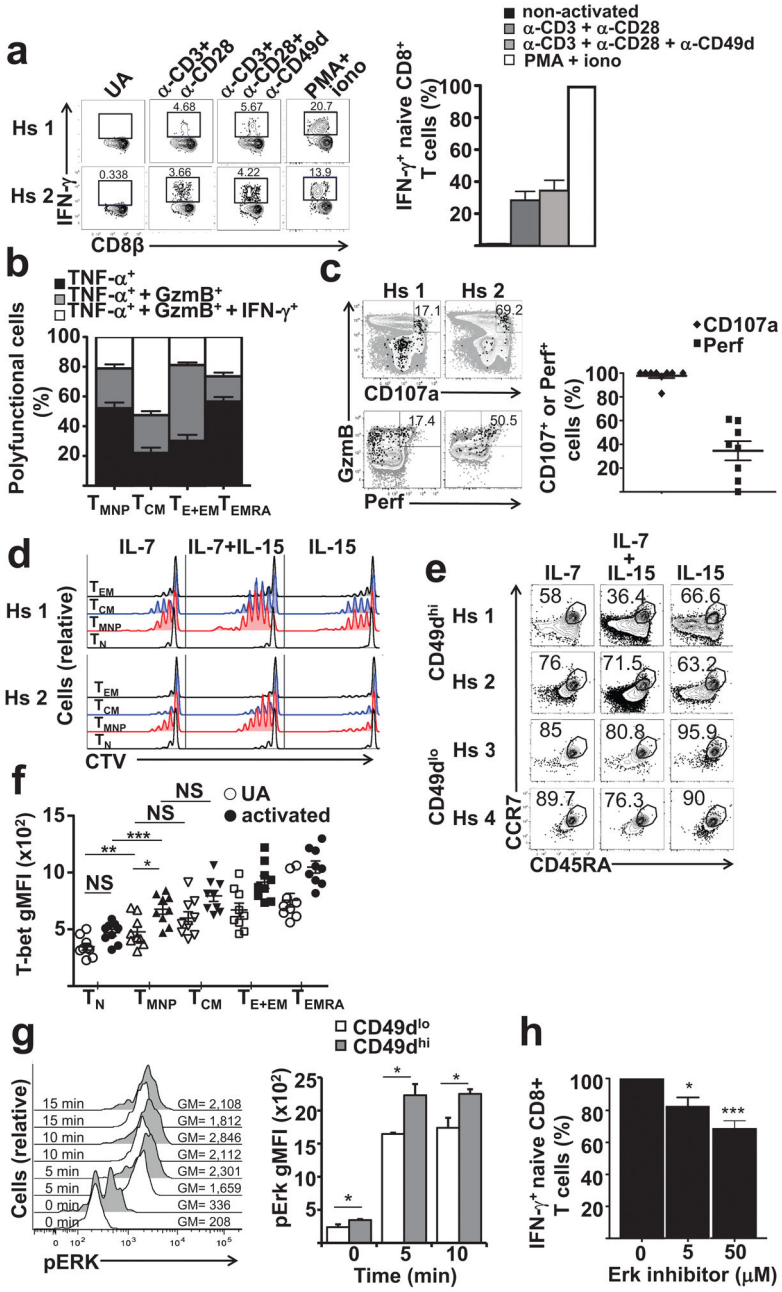

Figure 4. T_{MNP} cells show signs of prior activation

a. $CD8^+T_{MNP}$ cell % after 3h stimulation with indicated agonistic Ab (left) and as a fraction of PMA+iono response (±SD, n=10, 26–68y, repeated once). **b.** Intracellular cytokine expression by $CD8^+$T cell subsets (n=36, 24–82y). **c.** Left, 5% contour plots show representative degranulation ($CD107a^+$) and Perforin(Perf) production by IFN-$\gamma^+CD45RA^+CCR7^+CD95^{lo}CD28^{int}T_{MNP}CD8^+$ T cells (black) overlaid over total $CD8^+$ T cells (gray) (n=2, male, 52,63y of n=8, 31–77y, repeated twice). Right, cumulative frequencies of $CD107a^+$ and $Perf^+CD8^+T_{MNP}$ cells as percentage of IFNγ^+GzmB$^+T_{MNP}$ (n=8, 31–77y; repeated twice). **d.** Day 7 proliferation of sorted $CD8^+$ T cell subsets in

response to 50 ng/mL of IL-7 and IL-15 (subjects as in C; n=4/8 had all memory subsets as controls). **e.** Phenotype changes 3d after cytokine culture in 2 of 3 analyzed subjects (male, 52&64y). **f.** Mean gMFI±SEM of T-bet expression in different $CD8^+$ T cell subsets before or 2h after PMA+iono activation (significance by repeated measures one- way ANOVA between populations, ns= not significant, *p<0.05,**p<0.01, ***p<0.0001, n=9, 6 males, 3 females, age 27–78). **g.** Time course of pErk expression (right, gMFI shown) in T_{MNP} ($CCR7^+CD45RA^+CD95^{lo}CD28^{int}CD49d^{hi}$) vs T_N ($CCR7^+CD45RA^+CD95^{lo}CD28^{int}CD49d^{lo}$) $CD8^+$ T cells following 3h PMA+iono stimulation in a representative 68y old female. Left, mean pErk gMFI ±SD (repeated measures one-way ANOVA, n=3, 2 females, 1 male, of n=7, 67–83y,*p<0.05; repeated once). **h**. Dose-dependent decrease in IFN-**γ** production by PMA+iono stimulated $CD8^+$ T cells after pre-incubation with Erk inhibitor (n=14, 5f, 9m, 52–83y, repeated once). (Repeated measures one-way ANOVA; *p<0.05, ***p<0.0001).

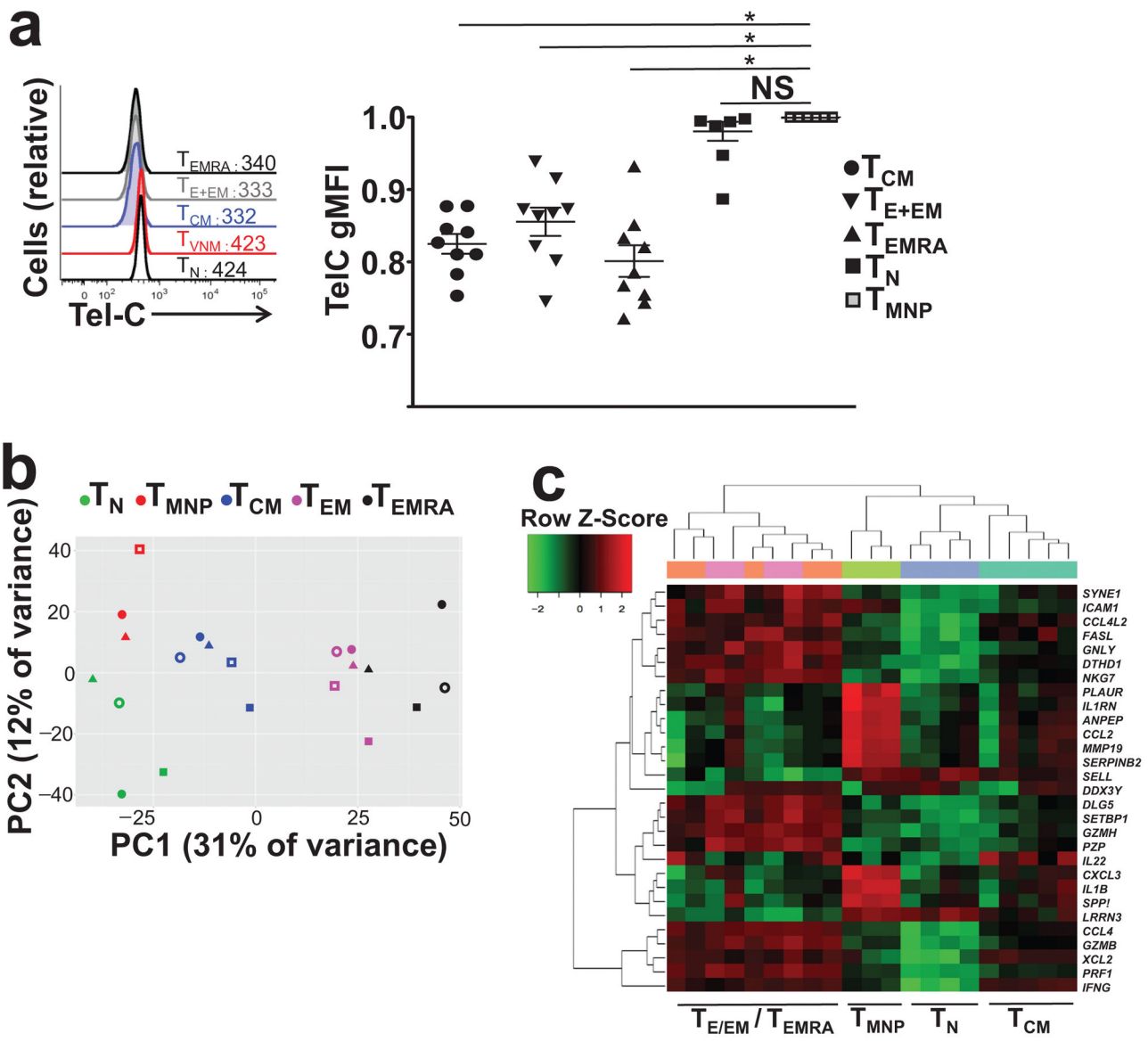

Figure 5. Telomere lengths and RNA transcriptome profile of T_{MNP} cells

a. Representative FACS plot analysis showing telomere length of different $CD8^+$ subsets (T_N ($CCR7^+CD45RA^+CD95^{lo}CD28^{int}$ $CD49d^{lo}$), T_{MNP} ($CCR7^+CD45RA^+CD95^{lo}CD28^{int}$ $CD49d^{hi}$), T_{CM}, T_{E+EM}, T_{EMRA}). Numbers indicate gMFI of Cy5 PNA telomere probe staining. Bar graph comparing telomere length of $CD8^+$ subsets with the length of naive subset within each individual (n=9, 6 females, 3 males, ages 34–83). **b.** Plot of the samples projected onto the first two principal components with variables of all Consensus Coding Sequence (CCDS) listed genes that were measured. The color distinguished the cell type (indicated in the figure legend) and shape distinguishes the subject from which the sample was derived. **c.** Heat map of differentially expressed genes (adjP<0.01, FDR<0.05. The expression values for each gene are standardized to a z-score and then binned to a color.

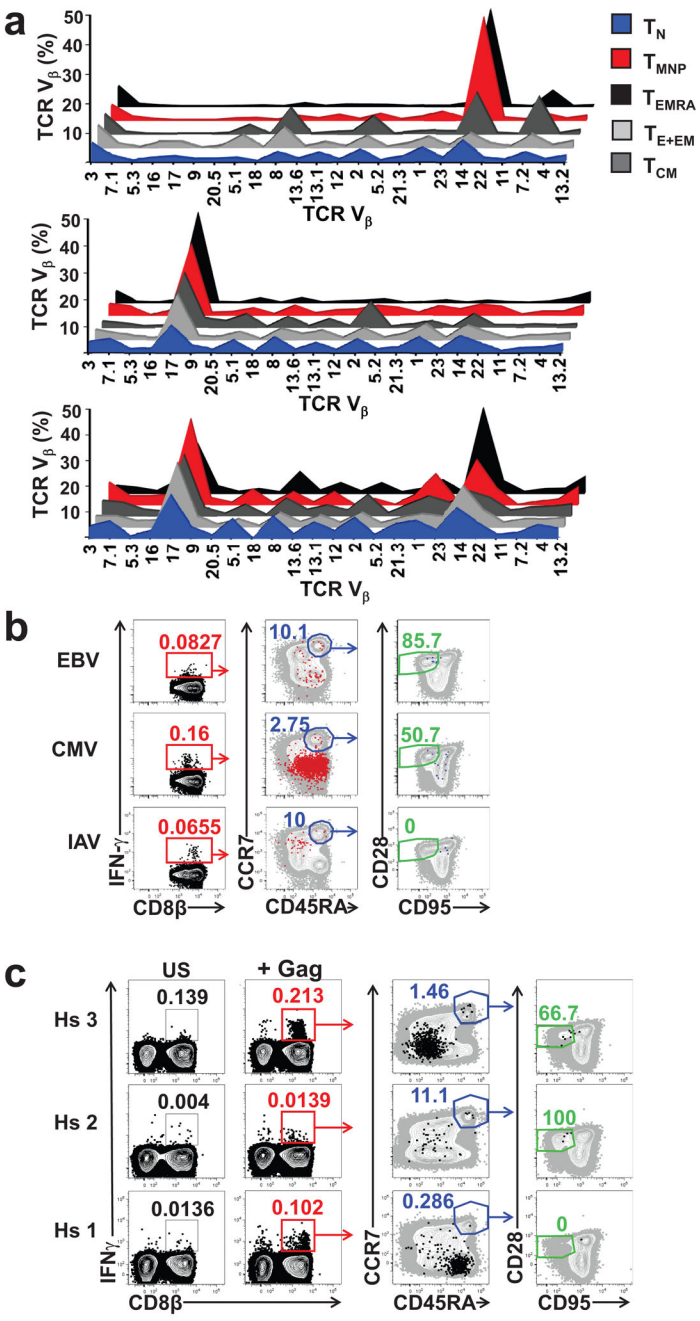

Figure 6. T_{MNP} cells have skewed TCR Vβ repertoire and can be detected among T cells responding to stimulation with EBV, CMV, and HIV peptides

a. 3D line graphs showing TCR Vβ distribution in different $CD8^+$ T cells subsets (T_N ($CD45RA^+$ $CCR7^+CD95^{lo}CD28^{int}CD49d^{lo}$), T_{MNP} ($CD45RA^+CCR7^+CD95^{lo}CD28^{int}$ $CD49d^{hi}$), T_{CM}, T_{E+EM} and T_{EMRA}) from 3 representative donors (of n=11, 6 males, 5 females, ages 27–78) shown as percentages of each of the 24 tested TCR Vβ (marked on the x axis) are shown. **b,c.** Flow cytometry analysis of PBMCs at 3 h after stimulation with **(b)** EBV BLZF1peptide pool, CMV pp65 peptide pool or IAV matrix protein peptide pool and **(c)** HIV (Gag) peptide pool. Dot plots show gating strategy to evaluate the naive phenotype

of the responding (IFN-γ producing) $CD8^+$ T cells. Numbers represent percentages of the population within each gate after subsequent gating (IFN-γ^+ $CD8^+$T cells followed by $CCR7^+CD45RA^+$ gate and subsequently by $CD95^{lo}$ $CD28^{int}$ gate). Total $CD8^+$ T cells are shown in gray. **(b)** Data are representative of one healthy donor with an n=8 (3 females, 5 males, ages 34–68) for each peptide stimulation; **(c)** Data show the response of three HIV+ ART donors with no detectable HIV in plasma.

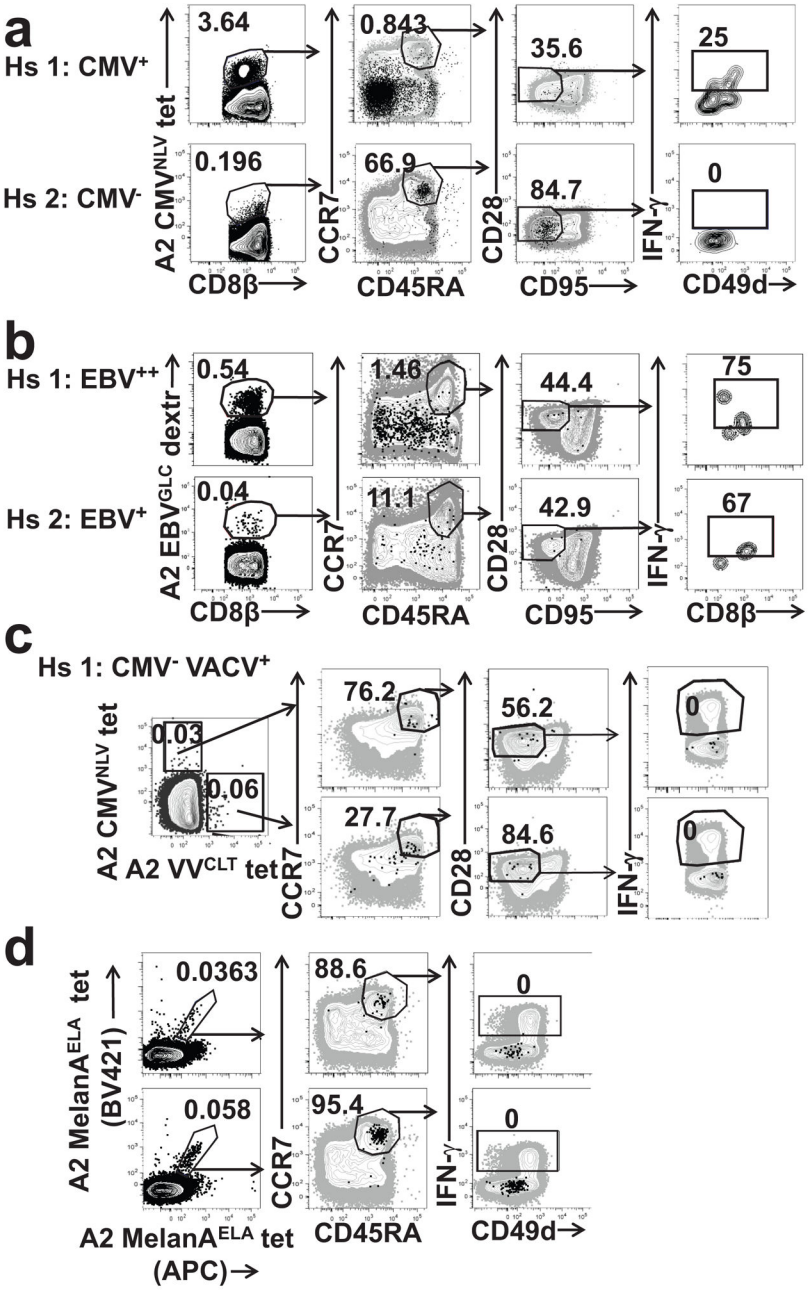

Figure 7. T_{MNP} cells are found among CMV and EBV -specific T cell pools and are not specific for influenza, smallpox, or self-antigens

a,b. Flow cytometry analysis of IFN-γ production by naive ($CD45RA^+CCR7^+CD95^{lo}CD28^{int}$) CMV **(a)** and EBV **(b)** specific $CD8^+$ T at 3 h after stimulation with PMA+iono. Four representative donors (one CMV seropositive (male, age 72) and one seronegative (female, age 65) and two EBV seropositive (males, ages 67 and 75) (high and low titer) of n=26, ages 28–83 (a) or n=7, ages 24–75) (b) are shown. Dot plots show gating strategy and the numbers represent percentages of the population within each gate after subsequent gating **c, d.** Flow cytometry analysis of IFN-γ production by naive ($CCR7^+CD45RA^+CD95^{lo}CD28^{int}$) vaccinia virus-specific $CD8^+$ T cells from two

representative donors (one CMV seropositive (female, age 64) and one seronegative (female, age 36) (of n=4, ages 36–74)) and naive Melan-A-specific $CD8^+$ T cells from two representative donors, females, ages 58 and 76 (of n=6, ages 29–82) after brief stimulation with PMA+iono (same gating strategy was used as in **a, b**). Data are representatives of one (a,b,c) and two (d) experiments.

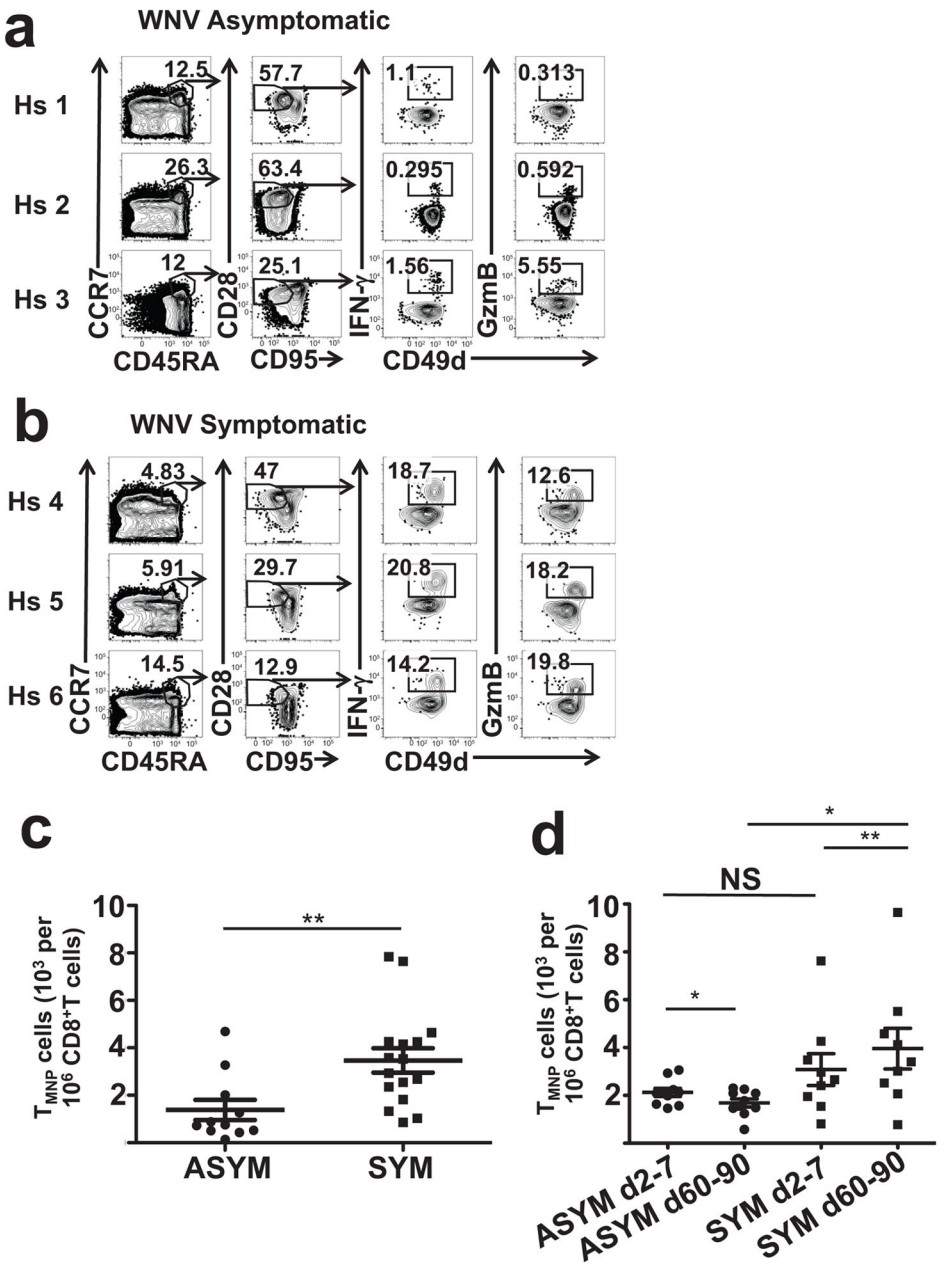

Figure 8. Individuals with symptomatic WNV infection show increased levels of T_{MNP} cells

a,b. Intracellular IFN-γ and GzmB staining of human PMA+iono- activated PBMCs from six representative WNV^+ donors (three WNV asymptomatic (**a**) and three WNV symptomatic (**b**)). Dot plots show gating strategy to quantify T_{MNP} ($IFN\gamma^+CD45RA^+CCR7^+CD95^{lo}CD28^{int}$) $CD8^+$ T cells (shown as percentages of the population within each gate after subsequent gating and quantified as number (mean ±SEM) of T_{MNP} cells per million $CD8^+$ T cells (**c**) (Mann-Whitney test, **p<0.01, n=26). Data are representative of one experiment). **d.** Quantification of T_{MNP} $CD8^+$ T cells (number (mean ±SEM) of T_{MNP} ($IFN\gamma^+CCR7^+CD45RA^+CD95^{lo}CD28^{int}$) cells per million $CD8^+$ T cells) from individuals with asymptomatic and symptomatic WNV infections early (day 2–7) and late (day 60–90)

after index donation (Repeated measures ANOVA was used to compare symptomatic group to asymptomatic group at two time points. Prior to applying repeated measures, equal variance assumption was tested by Levene's test. The heterogeneous Compound Symmetry covariance structure was used to not only account for the within subject correlation but also adjust for the variance heterogeneity. p=NS, *p<0.05, **p<0.01,(asymptomatic n=11, 39–92y old; symptomatic n=16, 43–84y). Data are representative of one experiment.